SCIENTIFIC REPORTS

OPEN

SUBJECT AREAS:
SELF-ASSEMBLY
SENSORS

Received
30 October 2013

Accepted
19 March 2014

Published
4 April 2014

Correspondence and requests for materials should be addressed to J.L.S. (sessler@cm.utexas.edu) or J.Y. (jyoon@ewha.ac.kr)

Anion-activated, thermoreversible gelation system for the capture, release, and visual monitoring of CO_2

Xin Zhang[1], Songyi Lee[1], Yifan Liu[1], Minji Lee[1], Jun Yin[1,2], Jonathan L. Sessler[3] & Juyoung Yoon[1]

[1]Department of Chemistry and Nano Science and Department of Bioinspired Science, Ewha Womans University, Seoul 120-750, Korea, [2]Key Laboratory of Pesticide and Chemical Biology, Ministry of Education, College of Chemistry, Central China Normal University, Wuhan 430079, P. R. China, [3]Department of Chemistry, 125 E. 24th Street-Stop A5300, The University of Texas at Austin, Austin, Texas 78712-1224, United States.

Carbon dioxide (CO_2) is an important green house gas. This is providing an incentive to develop new strategies to detect and capture CO_2. Achieving both functions within a single molecular system represents an unmet challenge in terms of molecular design and could translate into enhanced ease of use. Here, we report an anion-activated chemosensor system, NAP-chol 1, that permits dissolved CO_2 to be detected in organic media via simple color changes or through ratiometric differences in fluorescence intensity. NAP-chol 1 also acts as a super gelator for DMSO. The resulting gel is transformed into a homogeneous solution upon exposure to fluoride anions. Bubbling with CO_2 regenerates the gel. Subsequent flushing with N_2 or heating serves to release the CO_2 and reform the sol form. This series of transformations is reversible and can be followed by easy-to-discern color changes. Thus, NAP-chol 1 allows for the capture and release of CO_2 gas while acting as a three mode sensing system. In particular, it permits CO_2 to be detected through reversible sol-gel transitions, simple changes in color, or ratiometric monitoring of the differences in the fluorescence features.

Carbon dioxide (CO_2) has been the subject of widespread discussion and considerable political debate due to its role as a green house gas[1–3]. CO_2 plays a central role in human physiology, including respiratory function, and is critical to the modern agricultural, food, and chemical industries. The importance and prevalence of CO_2 is providing an incentive to develop new methods that permit the rapid, quantitative and selective detection of this relatively inert gas[4–7]. Currently, methods for CO_2 detection include infrared spectroscopy, pH or Severinghaus electrodes, Gas chromatography, and, more recently, optical chemosensors[5,8–11]. Within the generalized chemosensor paradigm, optical CO_2 sensors based on either fluorescence or UV spectroscopies are particularly attractive. When appropriately designed such sensors have the advantage of simplicity, low-cost, high sensitivity and good selectivity; they are also amenable to automation and can permit real-time analyses[12–18]. Colorimetric approaches, wherein changes in color and associated UV/vis spectral differences are used to indicate the presence of CO_2, are particularly attractive because, at least in principle they can permit detection using the unaided eye. Were such sensing combined with an ability to effect reversible CO_2 capture, it could allow the monitoring and sequestration of CO_2 to be combined. This could translate into increased ease of use and eventual cost savings if deployed in the field. To our knowledge this dual function challenge has yet to be met.

In recent years, low-molecular-weight gelators (LMWGs) have been used to create sensing systems that respond to a variety of analytes, including chiral compounds[19,20], anions[21–30], pH, and metal ions[31,32]. However, to the best of our knowledge, no gelation-based system is available that allows for the detection of CO_2. On the other hand, Weiss and coworkers reported a type of "latent" ammonium carbamate LMWG for the capture and release of CO_2 based on the reaction of a long-chain-alkylamine with CO_2 via a thermoreversible organogelation process[33]. Therefore, by combining a fluorophore or chromophore with an appropriate gelating system, it should be possible to develop a new approach for CO_2 detection that would allow sensing to be combined with capture. Here, we detail one approach to meeting this challenge. As detailed below, it is based on a combination of anion-induced deprotonation, reaction with CO_2, and gelation.

Recently, our group reported a novel fluoride ion-activated strategy for the detection of CO_2 involving a fluorescent and colorimetric benzobisimidazolium-based chemosensor[17]. Prior to our report, Gunnlaugsson

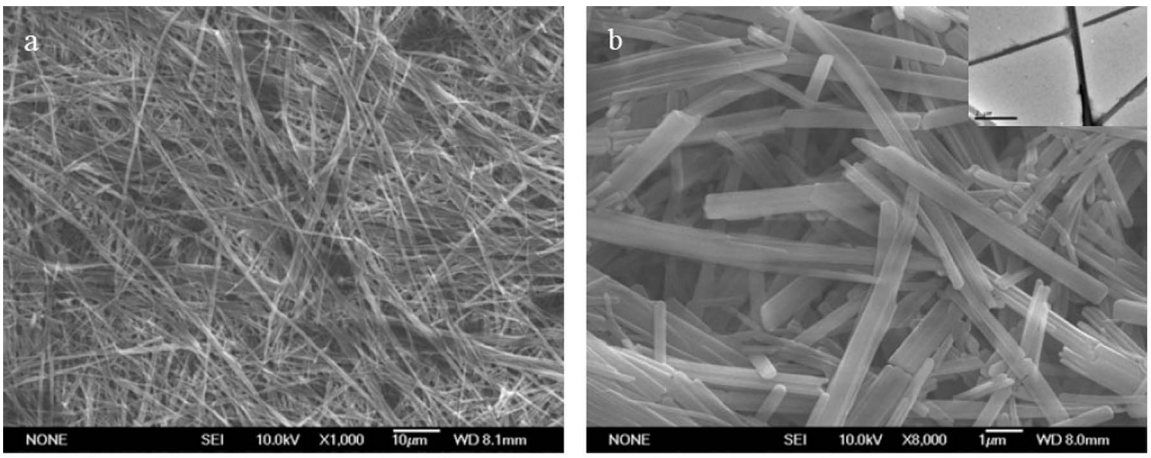

Figure 1 | SEM images of the xerogel obtained by drying DMSO solutions containing NAP-chol 1 (4 mg/ml) under vacuum at room temperature using a Pt backing (scale bar: (a) = 10 μm; (b) = 1 μm). The inset in Figure (b) shows the TEM image recorded for a xerogel sample obtained by drying a diluted DMSO solution of gelator **1** in the same manner but on a carbon-coated copper grid (scale bar: 1 μm).

and coworkers had found that naphthalimide amine derivatives could capture CO_2 in the presence of fluoride ion (F^-) via fluoride-induced deprotonation of the amine followed by reaction with CO_2[34]. These findings led us to consider that other acidic nitrogen derivatives, including amides and carbamates, could be used to create anion-activated fluorescent or colorimetric CO_2 sensing systems[35,36]. To test this hypothesis, we have prepared a new naphthalimide derivative, namely NAP-chol **1**. This system bears a cholesteryl moiety and a carbamate ester linker. 1,8-Naphthalimide is a versatile chromophore and fluorophore that has been extensively used in the design of colorimetric or fluorescent sensors. It possesses excellent photophysical properties, including a high molar extinction coefficient, a large fluorescent quantum yield and good photostability[37,38]. The corresponding carbamate ester can also serve as a hydrogen bond donor and, indeed, this moiety has been exploited to create anion receptors[36]. We thus reasoned that NAP-chol **1** would interact with anions and CO_2 in its neutral and deprotonated forms, respectively. This system also acts as a good gelator[39]. It thus allows for CO_2 detection through three distinct means, *i.e.*, reversible sol-gel transitions, ratiometric monitoring of absorption and emission spectral differences, and direct color changes. This system also permits the anion-triggered capture and release of CO_2.

Results and Discussion

Synthesis and gelation of NAP-chol 1. The synthesis of NAP-chol **1** is outlined in Supplementary Fig. S1. Briefly, 4-nitro-1,8-naphthalic anhydride is reacted with n-butylamine to produce **2**. The resulting nitro compound **2** is then reduced with hydrazine hydrate catalyzed by Pd/C to give the amino derivative **3**. Compound 3 and cholesteryl chloroformate were then coupled in dioxane under reflux to give NAP-chol **1** in an overall yield of 48%.

The ability of NAP-chol **1** to act as a gelator was tested by placing a small quantity (5.0 mg) in vials treating with a solvent (1.0 mL), heating until NAP-chol 1 was dissolved completely, and then cooling to room temperature (Supplementary Tab. S1). The vials were then inverted. If no appreciable flow to the bottom of the vial was observed, gelation was considered to have occurred. Out of the 22 solvents tested in this way, it was found that only dimethylsulfoxide (DMSO) would gelate NAP-chol **1**. Heating to above 60°C then served to reproduce the original sol form.

Notably, NAP-chol **1** shows a very low critical gelation concentration (CGC, the minimum concentration for the gelator to entrap solvents) of 0.18 wt% in DMSO. On that basis, it should be considered a so-called supergelator (CGC $<$ 1 wt%). For NAP-chol **1**, the sol-gel cycling process could be repeated more than 100 times without appreciable loss in integrity. On this basis, we propose that mixtures of NAP-chol **1** in DMSO constitute a thermally stable gelation system.

In addition to being readily formed and reformed on thermal cycling, the gels generated from NAP-chol **1** and DMSO proved robust, opaque and stable for several weeks at room temperature. Not surprisingly, the stability of the NAP-chol **1**/DMSO gel was found to increase as the gelator concentration increases. This concentration dependence is reflected in the different gel-to-sol transition temperatures (*T*g) obtained using different concentrations of the gelator. For instance, for concentrations of NAP-chol **1** in DMSO of 2, 3, and 5 mg/ml, respectively, *T*g values of 42, 49, and 61°C were recorded.

The morphology of the three-dimensional (3D) xerogel network obtained from the organogelator NAP-chol **1** was examined using scanning electron microscopy (SEM) and transmission electron microscopy (TEM). As shown in Fig. 1a, a well-defined 3D network structure involving in the entanglement of countless strip-like fibrous aggregates was observed in the SEM images. The same sample preparation procedure was used to obtain the samples for the TEM analyses except that a carbon-coated copper grid was used. The resulting TEM image is shown in the inset to Fig. 1b. Inspection of this image provides support for the notion that the one-dimension (1D) rod-like fibril with a width of 80–160 nm and length of a few micrometers is being formed under the conditions of initial gelation and TEM analysis. It is thus concluded that the intertwined fibers that result from the self-assembly of NAP-chol **1** in DMSO account for the immobilized and solvent entrapped nature of the gel phase.

In principle, gelator NAP-chol **1** can support multiple supramolecular interactions, involving, e.g., intermolecular hydrogen bonding between the carbamate groups, π-π donor-acceptor interactions between adjacent naphthalene rings, and van der Waals interactions between the cholesteryl substitutent. Individually, or in concert, these could provide the driving force for gelation[40–43]. FT-IR and ^{1}H NMR spectroscopic studies were undertaken in an effort to determine the dominant factors that drive gelation in the case of NAP-chol **1** and DMSO. In the FT-IR spectrum of solid NAP-chol **1** recorded at room temperature a broad band at 3460 cm^{-1} assigned to the carbamate NH stretching vibration was observed (Supplementary Fig. S2), whereas a peak at 3329 cm^{-1} is seen in the corresponding xerogel; such observations are consistent with the presence of the intermolecular hydrogen bonding interactions in the gel phase[44]. Furthermore, the concentration-dependent ^{1}H NMR spectral changes observed in $CDCl_3$ (Supplementary Fig. S3) revealed that an increase in the concentration of NAP-chol **1** leads to

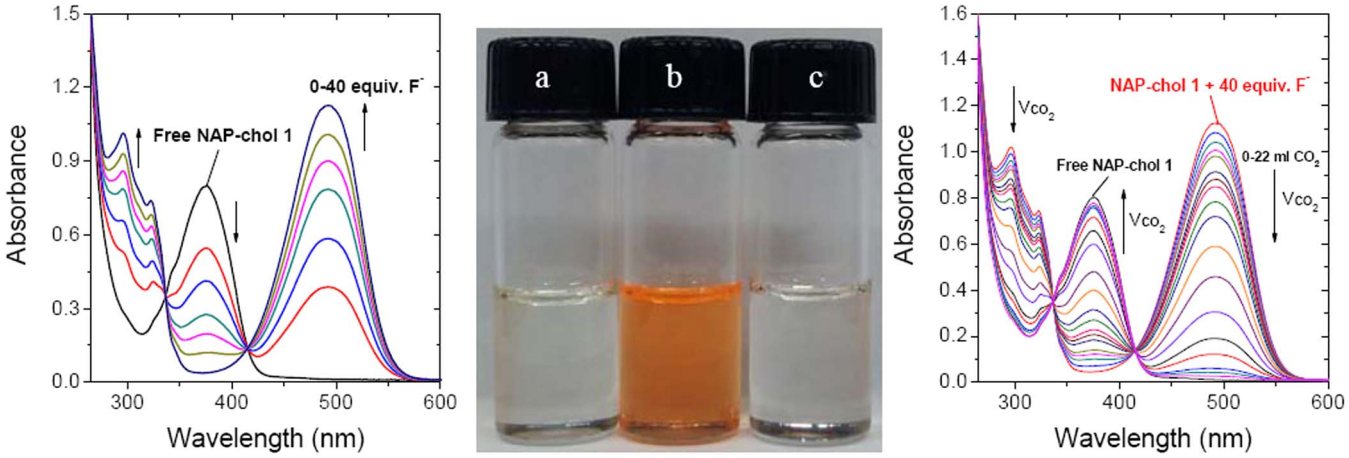

Figure 2 | UV/Vis spectral changes of sensor NAP-chol 1 (2.5×10^{-5} M in DMSO) observed in the presence of tetrabutylammonium fluoride (TBAF) and CO_2. Left: Spectra recorded upon the addition of different quantities of TBAF (0–1.0×10^{-3} M); right: Spectra recorded upon bubbling with different volumes of CO_2 in the presence of 40 equiv. of TBAF (1.0×10^{-3} M) at 25°C. Middle: Photograph showing the color changes corresponding to the UV spectral differences: (a) NAP-chol **1**; (b) NAP-chol **1** + TBAF; (c) NAP-chol **1** + TBAF + CO_2.

a downfield shift (from δ = 7.39 to 7.44 ppm) for the signals ascribed to the carbamate NH protons. Concurrently, the naphthalene ring proton signals are seen to shift upfield slightly, an observation rationalized in terms of an increase in the aromatic electron density due to the enhancement of the hydrogen bonding interactions between the carbamate ester groups. Temperature-dependent ^{1}H NMR spectra of the gel (Supplementary Fig. S4) recorded in DMSO-d_6 at a concentration of 2.8 mg/ml revealed that the NH resonance signals shift gradually upfield (from δ = 10.28 to 9.86 ppm) as the temperature increases from 25 to 95°C. This is taken as an indication that hydrogen bonding interactions may play a role in gel formation. Increasing the temperature also led to a slight upfield shift for the aromatic proton signals corresponding to the naphthalene rings. Such observations provide support for the existence of π-π interactions involving the naphthalene moieties within the gel state. These proposed π-π interactions account for the red shift in the absorption and fluorescence features of NAP-chol **1** seen in the gel phase as compared to what is observed in solution (Supplementary Fig. S9)[24,26]. Upon heating the deuterated DMSO-derived gel produced from NAP-chol **1**, the ^{1}H NMR spectral signals of the cholesteryl hydrogen atoms are seen to shift slightly downfield (e. g., from δ = 0.67 ppm at 25°C to 0.7 ppm at 95°C). More likely, however, the gross changes in morphology during the gel-sol transition simply serve to adjust the distance between, and magnetic environment of, these two hydrophobic moieties. Taken in concert, the above results lead us to suggest that intermolecular hydrogen bonding is the major driving force leading to fibril formation when NAP-chol **1** is mixed with DMSO, although other interactions may play an ancillary role in defining the structure.

Spectroscopic response of NAP-chol 1 toward CO_2 at low concentrations in solution. Intramolecular charge transfer (ICT) effects appear to play an important role in terms of defining the optical features of NAP-chol **1**. Such a suggestion is consistent with the D-π-A structure wherein the imide and the carbamate are expected to serve as the charge acceptor and donor, respectively[35]. This proposition is also supported by the observed solvatochromic behavior[45]. In particular, a slight red-shift is seen in the UV/Vis absorption maximum of NAP-chol **1** as the solvent polarity increases (Supplementary Fig. S5). In the case of the emission spectra of NAP-chol **1**, more distinct bathochromic shifts are seen as the polarity increases (Supplementary Fig. S5b). These results lead us to suggest that either the ground or the excited state of NAP-chol **1** can be tuned by application of stimuli that tune the effective local polarity. To the extent this supposition proved correct, the ICT feature of NAP-chol **1** were expected to allow this system to be exploited as an effective colorimetric and fluorescent ratiometric sensor. As detailed below, this proposition could be effectively realized when Lewis basic anions and CO_2 were used as the external stimuli.

Prior to studying NAP-chol **1** as a gel-based sensor for CO_2, we felt it important to analyze its reactivity behavior in solution. Since anion-induced deprotonation is considered to be a prerequisite for interaction with CO_2, our initial analyses involved recording the UV/Vis absorption spectral changes of NAP-chol **1** in the presence of varying concentrations of tetrabutylammonium fluoride (TBAF) in DMSO (2.5×10^{-5} M) at ambient temperature (Fig. 2 left). In the absence of TBAF, NAP-chol **1** exhibits an absorption band centered at 376 nm ($\varepsilon = 33{,}070\ M^{-1}\ cm^{-1}$). Upon the addition of TBAF up to 1.0×10^{-3} M, a new absorption band is observed with an absorption maximum at 493 nm ($\varepsilon = 46{,}064\ M^{-1}\ cm^{-1}$). The growth of this latter feature is accompanied by a decrease in the intensity of the 376 nm band. Two isosbestic points at 336 nm and 415 nm are also observed, as would be expected for a reaction where only two species are interconverting. Deprotonation of the carbamate moiety by the F^- ion is considered responsible for the new absorption band. Presumably, the buildup of increased negative charge on the nitrogen atom enhances the magnitude of the charge transfer effect[35]. Further spectroscopic studies revealed that NAP-chol **1** displayed selectivity for the fluoride anion over other representative anions (as the corresponding TBA^+ salts), including the cyanide ion (Supplementary Fig. S6).

We hypothesized that the addition of CO_2 can lead to complete or partial reprotonation of the carbamate moiety present in NAP-chol **1**[34,46]. This, in turn, would be expected to reduce the ICT effect noted above, leading to a blue-shift in the absorption spectral features of NAP-chol **1**. To test this assumption, a DMSO solution of NAP-chol **1** (3.0 ml; 2.5×10^{-5} M) containing 40 equiv. of TBAF was bubbled with CO_2 gas. As the volume of CO_2 entering the solution increased (as modulated by a mass flow controller), the intensity of the absorption band centered at 376 nm was seen to increase, while that of the CT band (493 nm) decreased. After the addition of ca. 22 ml of CO_2 the intensity of the 376 nm band ($\varepsilon = 32{,}085\ M^{-1}\ cm^{-1}$) was nearly restored to the level seen for the free form of NAP-chol **1**.

The spectral changes induced upon exposure to TBAF and CO_2 could also be followed by the unaided eye. For instance, as shown in the middle panel of Fig. 2, the addition of F^- ions to a DMSO solution of NAP-chol **1** induced a change from colorless to orange.

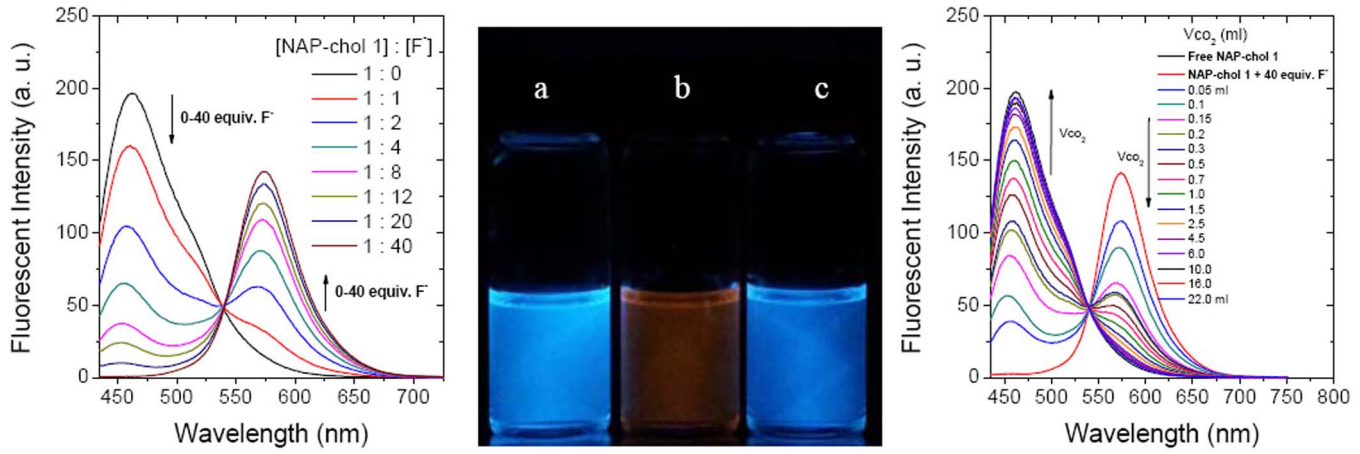

Figure 3 | Fluorescent features of sensor NAP-chol 1 (2.5×10^{-5} M) in DMSO seen in the presence of tetrabutylammonium fluoride (TBAF) and CO_2 upon excitation at 425 nm. Left: Fluorescence spectra recorded upon the addition of different quantities of TBAF (0–1.0×10^{-3} M); right: Fluorescence spectra recorded upon bubbling with different volumes of CO_2 in the presence of 40 equiv. of TBAF (1.0×10^{-3} M) at 25°C. Middle: Photographs recorded under a UV lamp; these correspond to the fluorescent spectral changes shown in the left and right panels: (a) NAP-chol **1**; (b) NAP-chol **1** + $TBAF^-$; (c) NAP-chol **1** + $TBAF^-$ + CO_2.

Subsequent exposure to CO_2 gas caused the solution to fade back to colorless.

The response of NAP-chol **1** toward the fluoride anion (as TBAF) and CO_2 in DMSO led to easy-to-discern changes in the fluorescence emission features. As shown in Fig. 3 left, when excited at 425 nm significant changes in the fluorescence features of NAP-chol **1** were observed upon the addition of F^-, including quenching of the 462 nm band and an increase in the intensity of the feature at 574 nm assigned to an ICT emission. Again, the changes could be followed by eye. For instance, under illumination with a 365 nm UV lamp the blue fluorescent solution of NAP-chol **1** fluoresces weakly orange after treating with 40 equiv. of TBAF (middle photograph of Fig. 3). When this latter solution was treated with CO_2 gas, the putative fluoride-induced ICT emission at 574 nm was quenched. Concurrently, the intensity of the 462 nm feature increases (Fig. 3 right).

The above spectroscopic changes in DMSO allow CO_2 sensing to be carried out ratiometrically. Specifically, a linear correlation between the CO_2 volumes (0–1.0 ml) and the intensity of the ratios of the 462 and 574 nm emission features (I_{462}/I_{574}), could be established (Supplementary Fig. S8). Based on the calibration curve obtained from this correlation, CO_2 detection limit of 0.03 bar (I_{462}/I_{574}) could be calculated for emission detection. In addition, the similar spectroscopic changes could be also observed in other organic solvents. For instance, when a polar organic solvent, dioxane, was used, the colorimetric and emission ratiometric responses were also observed upon the reaction of NAP-chol **1** with F^- ions and CO_2 (Supplementary Fig. S12, S13). On this basis, the CO_2 detection limit was calculated as 0.044 bar (I_{445}/I_{567}) (Supplementary Fig. S14).

To gain further understanding into the CO_2 sensing process, ^1H and ^{13}C NMR spectroscopic experiments were carried out in DMSO-d_6. As shown in Fig. 4, the addition of 8.0 equiv. of TBAF to NAP-chol **1** in this solvent led to the disappearance of the signal at 10.28 ppm ascribed to the carbamate N-H proton. This change, ascribed to deprotonation of the carbamate NH proton, was accompanied by the emergence of a new weak, broad signal at 16.17 ppm ascribed to formation of the bifluoride anion (HF_2^-)[47,48]. The subsequent exposure of the deprotonated form of NAP-chol **1** to excess CO_2 induced almost complete recovery in the chemical shifts of all the protons on the naphthalene ring, restoring them to the positions seen for neutral NAP-chol **1**. Near complete recovery of the chemical shifts of all carbons was also observed in the ^{13}C NMR spectrum (Supplementary Fig. S17). These results are consistent with the observed optical changes and support the suggestion that a deprotonated NAP-chol **1** species is formed upon fluoride treatment that then reacts with CO_2[49]. As can be seen from an inspection of Fig. S17, the ^{13}C NMR spectrum recorded after treatment with CO_2 revealed a new peak at 160.7 that is assigned to the carbon atom of the bicarbonate (HCO_3^-) anion[49]. Upon addition of CO_2, the sharp resonance originally seen for the residual water signal in the ^1H NMR spectrum becomes broadened. On this basis, we infer that the trace levels of water in the DMSO-d_6 solvent are involved in the underlying reactions with CO_2 (Supplementary Fig. S18).

A summary of the chemistry underlying the sensing process is shown in Fig. 4 (cf. right hand scheme). The whole process is reversible with CO_2 release being seen upon bubbling with N_2 gas at 50°C. As can be seen from an inspection of Fig. 4d, this N_2 bubbling restores the entire ^1H NMR spectrum of deprotonated form of NAP-chol **1**. No evidence of degradation is seen.

Gel-based CO_2 sensing upon anion activation. Based on the above predicative studies, it was expected that the gel formed between NAP-chol **1** and DMSO would provide an optical response upon exposure to anions or CO_2. As shown in Fig. 5, both the gel and sol forms give rise to blue-green fluorescence upon irradiation with a 365 nm UV lamp. However, the gel form of NAP-chol **1** gives rise to an emission maximum at 502 nm that is bathochromically shifted compared to what is seen in DMSO solution at low concentrations (Supplementary Fig. S9b and S9c). The fluorescence of NAP-chol **1** in the gel phase is also ca. 5-fold higher than in the sol state in DMSO (Supplementary Fig. S9c). These effects are ascribed to π-π donor-acceptor interactions between the vicinal naphthalene rings (*J*-aggregation)[26,50]. On the other hand, the addition of TBAF led to a gradual collapse in the integrity of the gel form. This transformation is accompanied by a color change from yellow-green to orange-red and complete conversion to a homogeneous solution within 1 h. Similar changes were seen when CN^- (as TBACN) was used instead of F^- (Supplementary Fig. S10 and S15). These results are further consistent with the suggestion made above that hydrogen bonding interactions play a key role in stabilizing the gel form. Presumably, Lewis basic anions such as F^- and CN^-, compete with the carbonyl group of the carbamate ester linker for the carbamate proton; this leads to a breakup of the hydrogen-bonded network that stabilizes the gel in their absence. Consistent with this view and the resulting ICT effects is the finding that a shift in the emission from blue-green to orange is observed upon gel collapse. Support for this conclusion is provided by the NMR spectral analyses discussed above.

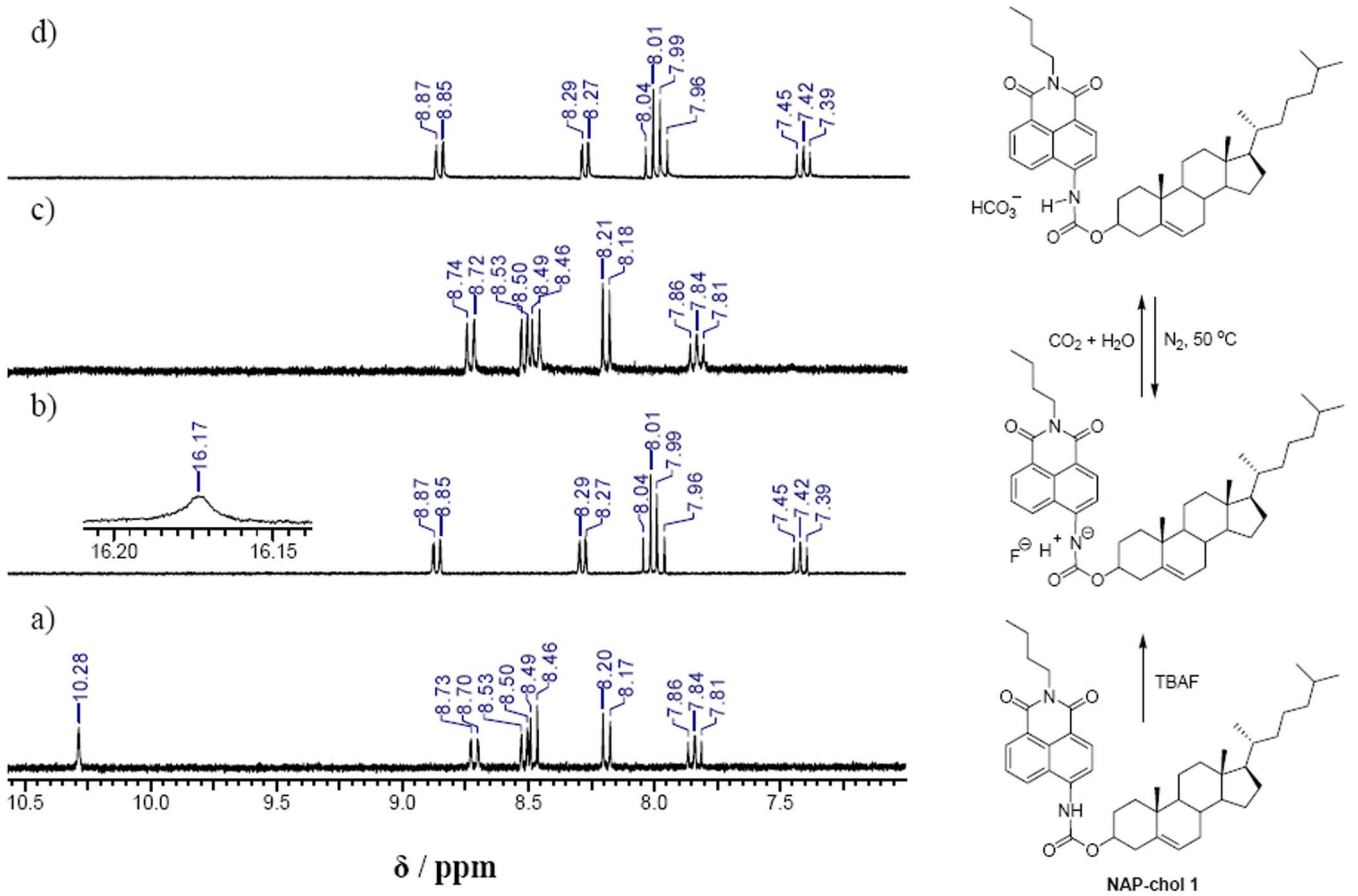

Figure 4 | Left: Partial views of the changes in the ^{1}H NMR (300 MHz) spectrum of NAP-chol **1** in DMSO-d_6 (0.4 mM) seen upon the addition of tetrabutylammonium fluoride (TBAF) and CO_2. (a) Free NAP-chol **1**; (b) after adding 8.0 equiv of TBAF; (c) bubbling with excess CO_2 in the presence of TBAF; (d) subsequent bubbling with N_2 at 50°C after (c). Right: Chemical reactions involving NAP-chol **1**, fluoride ion, and CO_2 that underlie the proposed sensing process.

To test the effect of CO_2 the sol phase produced by treating the DMSO-derived gels of NAP-chol **1** with excess F^- or CN^- (as the TBA^+ salts) was treated with CO_2 at room temperature. Upon bubbling with CO_2 the solution turned viscous and in due course gel-like rafts, some of which moved up along the inner wall of the vial pushed by the foaming action induced by bubbling. After 30 min CO_2 bubbling with the flow velocity of 3.0 ml/min, the vials in question were sealed and dipped in a hot water bath (50–55°C), then the formed red solution was cooled to room temperature. Under these conditions, an orange-yellow opaque gel is obtained that is characterized by a yellow-green fluorescence emission. Notably, the presence of either 8 or 40 equiv. of TBAF does not impact the gel recovery under the same conditions. Moreover, the reformed gels can be kept for several weeks without any evidence of collapse (Supplementary Fig. S16). The SEM images of the CO_2-induced DMSO gel (4 mg/ml) in the presence of 20 equiv. of TBAF (Fig. 6) reveal a visible network structure composed of countless entangled thread-like aggregates, which should be responsible for the re-gelation of the DMSO solvent. The reformed fibrils were evaluated by TEM. This analysis revealed fibers with a width of 60–110 nm and length of a few micrometers (Insets to Fig. 6). Based on the NMR spectral results (*vide supra*), recovery of neutral NAP-chol **1** is attributed to the gel regeneration with concomitant trapping of DMSO solvent.

Efforts were made to determine the minimum used amount of CO_2 needed for regeneration of the gel form of NAP-chol **1**. This value is not absolute. Rather it is a function of the amount of anion and NAP-chol **1** concentration. For instance, the lowest bubbling volume of CO_2 (at a flow rate of 3.0 ml/min) needed to effect gel regeneration for a 0.1 ml volume of a 4 mg/ml solution of NAP-chol **1** in DMSO in the presence of 8.0 equiv. of TBAF was found to be 0.09 ml (0.9 bar) at 25°C. Under the same conditions, the minimum quantities of CO_2 needed to regenerate 0.5 ml, 0.8 ml, and 1.0 ml samples of identical gelator-DMSO solutions were found to be 0.4 ml (0.8 bar), 0.75 ml (0.94 bar), and 0.95 ml (1.5 bar), respectively. In the presence of 4.0 equiv. of TBAF, the minimum CO_2 quantities could be decreased to 0.06 ml (0.6 bar), 0.23 ml (0.46 bar), 0.45 ml (0.53 bar), and 0.52 ml (0.82 bar), respectively, for otherwise identical 0.1, 0.5, 0.8, and 1.0 ml samples of the gelator solution.

Efforts to quantify the capturing efficiency (FE) of the NAP-chol **1** system were also made. The FE (% weight of captured CO_2/weight of total bubbled CO_2) was estimated by determining the weight increase of the overall system. Again, this was found to depend on the specific conditions. For instance, when CO_2 was bubbled into a DMSO solution of NAP-chol **1** (4 mg/ml) containing 8.0 equiv. of TBAF (conditions under which gel-like rafts were formed gradually), a greater increase in the overall weight of this system was seen than in the absence of NAP-chol **1**. Under these conditions and using a monitoring time of 60 min (a time point at which appreciable weight increases had ceased), a capturing efficiency of 30.1% was calculated for NAP-chol **1** as compared with 26.7% for a corresponding TBAF-DMSO control system (Supplementary Fig. S19).

As proved true in solution, CO_2 could be released from the gel produced from NAP-chol **1** by deprotonation and reaction with carbon dioxide could be realized by bubbling with N_2 at a temperature $>$ *T*g for the gel (42–48°C depending on the exact conditions and anion used). This bubbling serves to produce a red transparent

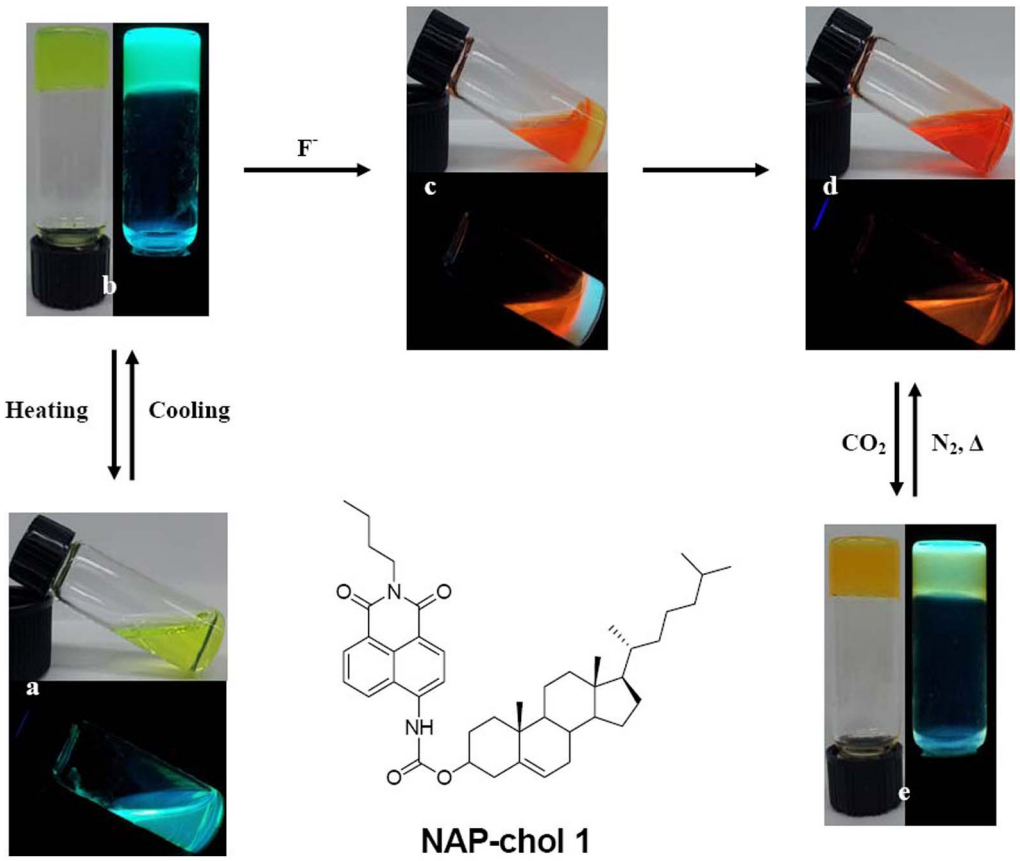

Figure 5 | Multiple responses of NAP-chol 1 (4 mg/ml) in DMSO under the stimulations of thermal, fluoride anions, and CO_2. (a) Sol; (b) Gel; (c) Partial or (d) complete collapse of the gel induced by fluoride anions; (e) upon the reaction with CO_2 in the presence of fluoride anions (20 equiv.).

solution whose spectral features mimic what is seen prior to the addition of CO_2. On this basis we conclude that system NAP-chol **1** permits reversible CO_2 capture coupled with sensing function via gel formation and stimulus induced sol-gel transitions.

Conclusions

In conclusion, we suggest that NAP-chol **1** represents an interesting new CO_2 recognition system. It allows this key analyte to be quantified using classic solution phase fluorescent- and absorption-based spectral changes. It also permits qualitative detection via simple color changes that can be followed by one's unaided eye. In addition, and in marked contrast to other CO_2 sensing strategies of which we are aware, it also allows CO_2 to be monitored directly via sol-gel transitions. The easy-to-observe nature of the latter transitions leads us to propose that NAP-chol **1** and related systems could have a role to play analyzing for this all-important industrial and greenhouse gas. The convenience of being able to accomplish the key functions of CO_2 sensing and capture using one molecular entity (NAP-chol **1**) represents an advance in terms of molecular design and is one that, in due course, could translate into enhanced ease of use and cost savings

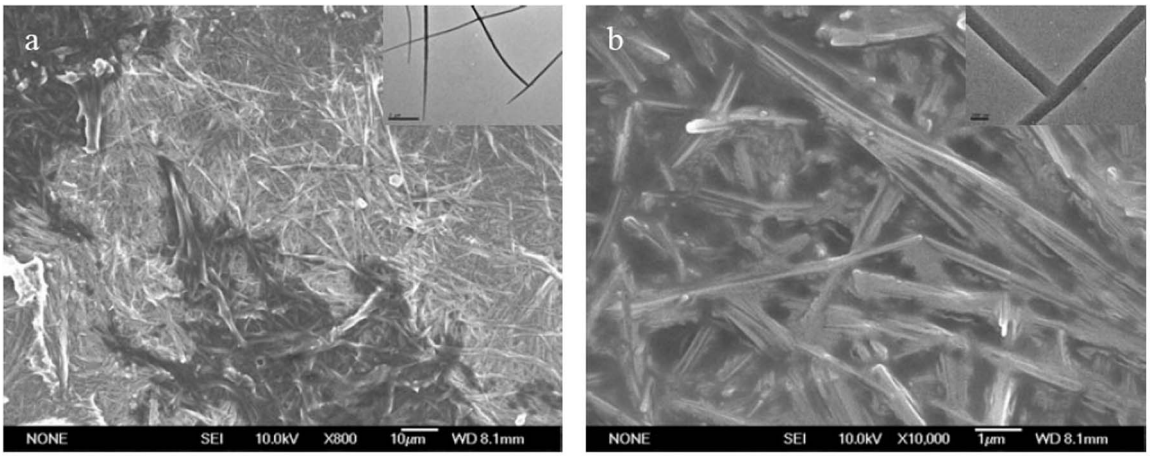

Figure 6 | SEM images of the xerogel reformed upon the reaction of NAP-chol 1 (4 mg/ml) in DMSO with CO_2 in the presence of 20 equiv. of the fluoride ion (as TBAF) (scale bar: (a) = 10 μm; (b) = 1 μm). Insets show the TEM images of the xerogel prepared from the diluted DMSO gel (scale bar: (a) inset = 1 μm; (b) inset = 100 nm).

when this or related systems are applied to the problem of carbon monoxide monitoring and sequestration.

Methods

CO_2 detection. If it is not otherwise indicated, all absorption and fluorescent experiments were carried out using 3 ml solutions of NAP-chol **1**. A stock solution of tetrabutylammonium fluoride was prepared in DMSO (0.1 M). 30 μl of the stock solution was added to 3.0 ml of the DMSO/NAP-chol **1** solution (2.5×10^{-5} M) giving the samples for the absorption and fluorescence tests. The concentration of the fluoride ions was 1.0 mM in the CO_2 detection experiments. A needle connected with a hose was inserted to the bottom of the sample solution for the purpose of CO_2 bubbling. A DFC-4000 digital flow controller connected to the source gas cylinder by a hose was used to modulate the velocity of the CO_2 flow. Absorption spectra were recorded in a 10 × 10-mm quartz cuvettes (HELLMA; type number 100-QS) on a Thermo Fisher Scientific Evolution 201 UV/Visible spectrophotometer under the control of a PC system (Windows 8) with the professional software supplied by the manufacturer. Fluorescence spectra were measured in a 10 × 10 mm disposable cuvette (HELLMA; type number 101.650-QG) on a RF-5301/PC spectrofluorophotometer (Shimadzu) controlled by a PC (Windows XP) running software provided by the manufacturer.

Gel characterization. The SEM images were determined from a field emission scanning electron microscope (JMS-6700F, JEOL) operated at 5.0 or 10.0 keV. The SEM samples were prepared by spreading the gel (consisting of NAP-chol **1** at 4 mg/ml in DMSO) on a glass sheet and drying at room temperature under vacuum for 24 h. The resulting xerogel was sputter-coated with 5 nm platinum in a Cressington 328 coating unit, at 40 mA. Transmission electron microscopy (TEM) images were obtained on a JEM-2100F TEM instrument operating at an acceleration voltage of 200 kV. TEM samples were prepared by depositing several drops of the diluted gel mixture onto standard carbon-coated copper grid, followed by drying under vacuum at ambient temperature for 24 h. For the CO_2-induced reformed gel, the solvent was volatilized at ambient temperature under atmospheric pressure for 1 week.

1. Schrag, D. P. Preparing to capture carbon. *Science* **315**, 812–813 (2007).
2. Li, L. *et al.* A review of research progress on CO_2 capture, storage, and utilization in chinese academy of sciences. *Fuel* **108**, 112–130 (2013).
3. Dawson, R., Cooper, A. I. & Adams, D. J. Chemical functionalization strategies for carbon dioxide capture inmicroporous organic polymers. *Polym. Int.* **62**, 345–352 (2013).
4. Perry, S. F. & Abdallah, S. Mechanisms and consequences of carbon dioxide sensing in fish. *Respir. Phys. Neurobiol.* **184**, 309–315 (2012).
5. Neethirajan, S., Jayas, D. S. & Sadistap, S. Carbon dioxide (CO_2) sensors for the agri-food industry–a review. *Food Bioprocess Technol.* **2**, 115–121 (2009).
6. Puligundla, P., Jung, J. & Ko, S. Carbon dioxide sensors for intelligent food packaging applications. *Food Control* **25**, 328–333 (2012).
7. Mills, A., Lepre, A. & Wild, L. Breath-by-breath measurement of carbon dioxide using a plastic film optical sensor. *Sens. Actuators, B* **38–39**, 419–425 (1997).
8. Yasuda, T., Yonemura, S. & Tani, A. Comparison of the characteristics of small commercial NDIR CO_2 sensor models and development of a portable CO_2 measurement device. *Sensors* **12**, 3641–3655 (2012).
9. Vorotyntsev, V. M., Mochalov, G. M. & Baranova, I. V. Gas chromatographic determination of admixtures of permanent gases, CO, CO_2, and hydrocarbons in methylsilane. *J. Anal. Chem.* **68**, 152–155 (2013).
10. Xie, X. & Bakker, E. Non-Severinghaus potentiometric dissolved CO_2 sensor with improved characteristics. *Anal. Chem.* **85**, 1332–1336 (2013).
11. Beyenal, H., Davis, C. C. & Lewandowski, Z. An improved Severinghaus-type carbon dioxide microelectrode for use in biofilms. *Sens. Actuators, B* **97**, 202–210 (2004).
12. Hampe, E. M. & Rudkevich, D. M. Reversible covalent chemistry of CO_2. *Chem. Commun.* 1450–1451 (2002).
13. Amao, Y. & Nakamura, N. Optical CO_2 sensor with the combination of colorimetric change of α-naphtholphthalein and internal reference fluorescent porphyrin dye. *Sens. Actuators, B* **100**, 347–351 (2004).
14. Amao, Y. & Komori, T. Optical CO_2 sensor of the combination of colorimetric change of α-naphtholphthalein in poly(isobutyl methacrylate) and fluorescent porphyrin in polystyrene. *Talanta* **66**, 976–981 (2005).
15. Wencel, D. *et al.* Ratiometric fluorescence-based dissolved carbon dioxide sensor for use in environmental monitoring applications. *Anal. Bioanal. Chem.* **398**, 1899–1907 (2010).
16. Dansby-Sparks, R. N. *et al.* Fluorescent-dye-doped sol-gel sensor for highly sensitive carbon dioxide gas detection below atmospheric concentrations. *Anal. Chem.* **82**, 593–600 (2010).
17. Guo, Z. *et al.* A benzobisimidazolium-based fluorescent and colorimetric chemosensor for CO_2. *J. Am. Chem. Soc.* **134**, 17846–17849 (2012).
18. Schutting, S., Borisov, S. M. & Klimant, I. Diketo-pyrrolo-pyrrole dyes as new colorimetric and fluorescent pH indicators for optical carbon dioxide sensors. *Anal. Chem.* **85**, 3271–3279 (2013).
19. Chen, X. *et al.* Enantioselective gel collapsing: a new means of visual chiral sensing. *J. Am. Chem. Soc.* **132**, 7297–7299 (2010).
20. Tu, T. *et al.* Visual chiral recognition through enantioselective metallogel collapsing: synthesis, characterization, and application of platinum–steroid low-molecular-mass gelators. *Angew. Chem. Int. Ed.* **50**, 6601–6605 (2011).
21. Lloyd, G. O. & Steed, J. W. Anion-tuning of supramolecular gel properties. *Nat. Chem.* **1**, 437–442 (2009).
22. Zhang, Y. *et al.* A novel smart organogel which could allow a two channel anion response by proton controlled reversible sol–gel transition and color changes. *Chem. Commun.* 6074–6076 (2009).
23. Teng, M. *et al.* Glycine-glutamic-acid-based organogelators and their fluoride anion responsive properties. *J. Mater. Chem.* **19**, 5648–5654 (2009).
24. Liu, J. *et al.* Novel anion-tuning supramolecular gels with dual-channel response: reversible sol-gel transition and color changes. *Langmuir* **26**, 9040–9044 (2010).
25. Kim, T. H., Kwon, N. Y. & Lee, T. S. Synthesis of organogelling, fluoride ion-responsive, cholesteryl-based benzoxazole containing intra- and intermolecular hydrogen-bonding sites. *Tetrahedron Letts.* **51**, 5596–5600 (2010).
26. Xu, D. *et al.* New dendritic gelator bearing carbazole in each branching unit: selected response to fluoride ion in gel phase. *Org. Biomol. Chem.* **9**, 1523–1528 (2011).
27. Lu, J. *et al.* A new dual-responsive organogel based on uracil-appended glycyrrhetinic acid. *Org. Lett.* **13**, 3372–3375 (2011).
28. Rajamalli, P. & Prasad, E. Low molecular weight fluorescent organogel for fluorideion detection. *Org. Lett.* **13**, 3714–3717 (2011).
29. Zhang, Y. & Jiang, S. Fluoride-responsive gelator and colorimetric sensor based on simple and easy-to-prepare cyano-substituted amide. *Org. Biomol. Chem.* **10**, 6973–6979 (2012).
30. Xing, L. *et al.* Reversible sol-to-gel transformation of uracil gelators: specific colorimetric and fluorimetric sensor for fluoride ions. *Langmuir* **29**, 2843–2848 (2013).
31. Liu, Q. *et al.* Structural characterization and chemical response of a Ag-coordinated supramolecular gel. *Langmuir* **23**, 8217–8223 (2007).
32. Deng, W. & Thompson, D. H. pH and cation-responsive supramolecular gels formed by cyclodextrin amines in DMSO. *Soft Matter* **6**, 1884–1887 (2010).
33. George, M. & Weiss, R. G. Chemically reversible organogels: aliphatic aminesas "latent" gelators with carbon dioxide. *J. Am. Chem. Soc.* **123**, 10393–10394 (2001).
34. Gunnlaugsson, T. *et al.* Simple naphthalimide based anion sensors: deprotonation induced colour changes and CO_2 fixation. *Tetrahedron Lett.* **44**, 8909–8913 (2003).
35. Liu, B. & Tian, H. A ratiometric fluorescent chemosensor for fluoride ions based on a proton transfer signaling mechanism. *J. Mater. Chem.* **15**, 2681–2686 (2005).
36. Wang, S. *et al.* A multiple switching bisthienylethene and its photochromic fluorescent organogelator. *Chem. Commun.* 1497–1499 (2006).
37. Duke, R. M. *et al.* Colorimetric and fluorescent anion sensors: an overview of recent developments in the use of 1,8-naphthalimide-based chemosensors. *Chem. Soc. Rev.* **39**, 3936–3953 (2010).
38. Xu, Z. *et al.* Zn^{2+}-triggered amide tautomerization produces a highly Zn^{2+}-selective, cell-permeable, and ratiometric fluorescent sensor. *J. Am. Chem. Soc.* **132**, 601–610 (2010).
39. George, M. & Weiss, R. G. Molecular organogels. soft matter comprised of low-molecular-mass organic gelators and organic liquids. *Acc. Chem. Res.* **38**, 489–497 (2006).
40. de Jong, J. J. D. *et al.* Reversible optical transcription of supramolecular chirality into molecular chirality. *Science* **304**, 278–281 (2004).
41. Sugiyasu, K., Fujita, N. & Shinkai, S. Visible-light-harvesting organogel composed of cholesterol-based perylene derivatives. *Angew. Chem. Int. Ed.* **43**, 1229–1233 (2004).
42. Dou, C. *et al.* Sonication-induced molecular gels based on mono-cholesterol substituted quinacridone derivatives. *Langmuir* **26**, 2113–2118 (2010).
43. Wu, J. *et al.* Ultrasound switch and thermal self-repair of morphology and surface wettability in a cholesterol-based self-assembly system. *Angew. Chem. Int. Ed.* **47**, 1063–1067 (2008).
44. Wu, J. *et al.* Gelation induced reversible syneresis via structural evolution. *J. Mater. Chem.* **19**, 3971–3978 (2009).
45. Ji, S. *et al.* Tuning the intramolecular charge transfer of alkynylpyrenes: effect on photophysical properties and its application in design of OFF-ON fluorescent thiol probes. *J. Org. Chem.* **74**, 4855–4865 (2009).
46. Mindrup, E. M. & Schneider, W. F. Computational comparison of the reactions of substituted amines with CO_2. *Chem. Sus. Chem.* **3**, 931–938 (2010).
47. Kang, S. O. *et al.* Trapped bifluoride. *Angew. Chem. Int. Ed.* **45**, 1921–1925 (2006).
48. Shenderovich, I. G. *et al.* Low-temperature NMR studies of the structure and dynamics of a novel series of acid-base complexes of HF with collidine exhibiting scalar couplings across hydrogen bonds. *J. Am. Chem. Soc.* **125**, 11710–11720 (2003).
49. Ishida, M. *et al.* Benzimidazole-embedded N-fused aza-indacenes: synthesis and deprotonation-assisted optical detection of carbon dioxide. *Chem. Commun.* **49**, 6950–6952 (2013).
50. Wang, M. *et al.* Fluorescence enhancement upon gelation and thermally-driven fluorescence switches based on tetraphenylsilole-based organic gelators. *Chem. Phys. Lett.* **475**, 64–67 (2009).

Acknowledgments

This work was also supported by the National Research Foundation of Korea (NRF) grant funded by the Korea government (MSIP) (No. 2012R1A3A2048814 to J.Y.). The work was also supported by the U.S. National Science Foundation (NSF) (no. CHE-1057904 to J.L.S.).

Author contributions

X.Z. and J.Y.* designed the experiments with input from J.L.S.*. X.Z. synthesized and characterized gelator NAP-chol **1**, and generated the data shown in Fig. 1–6. S.L. carried out the SEM determination. Y.L., M.L. and J.Y. participated in parts of spectroscopic tests. X.Z., J.L.S.* and J.Y.* wrote the manuscript.

Additional information

Supplementary information accompanies this paper at http://www.nature.com/scientificreports

Competing financial interests: The authors declare no competing financial interests.

How to cite this article: Zhang, X. *et al.* Anion-activated, thermoreversible gelation system for the capture, release, and visual monitoring of CO_2. *Sci. Rep.* **4**, 4593; DOI:10.1038/srep04593 (2014).